JOURNAL OF AIRCRAFT
Vol. 32, No. 6, November–December 1995

Correlation of F/A-18 Buffeting from Wind-Tunnel and Flight Tests

D. E. Bean* and B. H. K. Lee†
National Research Council, Ottawa K1A 0R6, Ontario, Canada

A method to predict full-scale buffet of the F/A-18 vertical tail using measurements taken on a rigid wind-tunnel model is presented. Tests were performed on a rigid 6% scale F/A-18 in the 1.5-m trisonic blowdown wind tunnel at the National Research Council in Ottawa, over a range of angle of attack and Mach number. The results from the prediction code were compared to flight test results, which were obtained from flights undertaken at the Aerospace Engineering Test Establishment in Cold Lake, Alberta. In general, comparisons between flight and scaled wind-tunnel data were good, although the initial prediction code invariably underpredicted the full-scale response. Through the use of a variable pressure correlation technique (based on flight conditions) the accuracy of the prediction model was significantly increased. The flight data was also reduced to the nondimensional buffet excitation parameter. It was found that buffeting in the fundamental torsional mode at approximately 45 Hz occurred at a lower angle of attack (with larger overall magnitudes) compared to the fundamental bending mode at 15 Hz.

Nomenclature

A	=	area
C	=	damping coefficient
$\bar{c}$	=	wing mean aerodynamic chord, 8.29 in.
$\bar{c}_f$	=	fin mean aerodynamic chord, 5.03 in.
f	=	frequency
g	=	acceleration due to gravity, 32.2 ft/s^2
H	=	transfer function
K	=	generalized stiffness
k	=	reduced frequency, $f\bar{c}/U$
l	=	generalized force
M, m	=	generalized mass
N	=	number of modes
$\sqrt{nG(n)}$	=	buffet excitation parameter
p	=	pressure
Q	=	spectrum of generalized displacement
q	=	generalized coordinate, dynamic pressure, psf
Re	=	Reynolds number based on wing mean aerodynamic chord
S	=	fin area, 26.6 in.^{2}
$S_{p_1p_2}$	=	cross-spectral density of pressures p_1 and p_2
S_l	=	cross-spectral density of generalized force
U	=	freestream velocity
x, y, z	=	fin coordinate system
$\ddot{z}$	=	rms acceleration
ζ	=	modal damping (fraction of critical)
ϕ	=	mode shape function
$\bar{\phi}$	=	average mode shape
ω	=	circular frequency

Subscripts

b, c	=	panel indices
D	=	forcing pressure distribution
i, j	=	mode indices
M	=	aeroelastic term

I. Introduction

VERTICAL tail buffeting has emerged as a major cause of envelope restrictions to combat aircraft operating at high angles of attack (AOA). The fatigue problems associated with the buffet have been especially common for twin-tail aircraft with wing leading-edge extension (LEX), such as the F/A-18.

Although recent research into buffet alleviation[1–3] has proved successful for existing aircraft that already exhibit buffet, the prediction of buffet remains a prime objective with regard to the design of future high-performance aircraft.

The methods used to predict buffet invariably entail the scaling of data obtained from wind-tunnel tests performed on either a flexible or rigid model. The flexible model may be dynamically scaled to match the properties of the full-size structure, and instrumented with strain gauges and accelerometers, so that scale buffet measurements are obtained immediately. However, this approach is expensive, time consuming, and may not be used early in the design phase. The rigid model approach comprises the measurement of oscillatory pressures on a rigid wind-tunnel model, and so may be suitable for the early design phase, providing that a finite element model of the full-scale structure is available. The advantage of the rigid model method is that structural properties can be modified if necessary to ensure load limits are met before the prototype is built.

Ferman et al.[4] performed a study of buffet scaling laws for both flexible and rigid F/A-18 data. For the flexible model data, scaling laws based on dimensional analysis yielded good approximations to the measured flight responses. Scaling of the unsteady pressures on the rigid fin/stabilator (incorporating aeroelastic terms into the prediction model) gave a fair comparison with the measured model response.

The aim of the present research program is to develop a method to predict full-scale buffet loads on an elastic aircraft from measurements taken on a rigid wind-tunnel model. The wind-tunnel tests were performed in the 1.5-m trisonic blowdown wind tunnel at the National Research Council, whereas

Presented as Paper 94-1800 at the AIAA 12th Applied Aerodynamics Conference, Colorado Springs, CO, June 20–23, 1994; received Aug. 2, 1994; revision received June 2, 1995; accepted for publication June 15, 1995. Copyright © 1995 by D. E. Bean and B. H. K. Lee. Published by the American Institute of Aeronautics and Astronautics, Inc., with permission.

*G-7 Summit Fellow, Institute for Aerospace Research. Member AIAA.

†Senior Research Officer, Institute for Aerospace Research, High Speed Aerodynamics Laboratory; also Adjunct Professor, Department of Mechanical Engineering, University of Ottawa, Ottawa, Ontario, Canada. Associate Fellow AIAA.

the flight test results have been obtained from flights undertaken at the Aerospace Engineering Test Establishment (AETE).

II. Wind-Tunnel Tests

A. Test Facility

Wind-tunnel tests were performed in the 1.5 × 1.5 m transonic test section of the Institute for Aerospace Research (IAR) trisonic blowdown wind tunnel. The facility has a Mach number range of 0.1–4.2, and a hydraulically driven control system ensures a Mach number accuracy of ±0.003 over the entire model pitch range. The stagnation pressure is maintained to an accuracy of ±0.02 psia throughout the wind-tunnel run.

The walls of the test section are perforated by 0.5-in.-diam holes inclined at 30 deg to the freestream direction, allowing pressure and flow communication between the test section and a 12-ft-diam, 16-ft-long plenum chamber. By means of sliding throttle plates, the wall porosity may be set in the range 0.5–6%. For the present tests the wall porosity was set to 4%.

Model support was achieved by a cranked sting connected to a vertically translating strut. The vertical motion of the strut may be controlled, so that a model angle-of-attack range of 0–33 deg is available. Sting bending under aerodynamic load resulted in approximately a 2-deg incremental pitch angle at the highest angle of attack for the Mach number range tested.

The tests were performed at four Mach numbers, namely, 0.25, 0.31, 0.38, and 0.44, for an angle-of-attack range of $21 < \alpha < 33$ deg. Test Reynolds numbers (based on the mean aerodynamic chord of the wing) and dynamic pressures for the tests were in the ranges $1.41 \times 10^6 < Re < 2.48 \times 10^6$ and $0.83 < q < 2.36$ psia, respectively. Test runs were typically 8–9 s per test point.

B. Model Design and Instrumentation

The model used for the tests was a rigid 6% scale F/A-18 (Ref. 3). The model consists of three major pieces, namely an aluminum alloy nose section, with integral LEX, removable LEX fences, and a single seat canopy; a stainless-steel center fuselage with integral wings; and a stainless-steel rear fuselage. The center fuselage section is bored to accept a 38.1-mm-diam Able Corporation, six-component sting balance.

Leading- and trailing-edge flaps are fastened to the wings by simple bolted lap joints, with dowel pins for accurate assembly. For the present model configuration the leading- and trailing-edge flap deflections were set to 35 and 0 deg, respectively, which are similar to those for the flight test aircraft at the corresponding flight conditions. All tests were conducted with the LEX fence on.

The vertical fins are fastened to a steel insert, which in turn, is bolted to the rear fuselage. The horizontal stabilators are clamped to a fitting that is fixed to the rear fuselage. The stabilator angle was set to −9 deg for this study.

Boundary-layer transition trips of 0.05-mm-high epoxy cylinders (1.1 mm diameter on 2.5 mm centers) were installed approximately 10.2 mm behind the leading edges of the LEXs, wings, intakes, vertical fins, and horizontal stabilators on each surface. A ring of trips was also mounted 10.2 mm behind the tip of the nose. In addition, trips were placed along the port and starboard sides of the forebody, from the nose to the engine intakes.

For these tests the starboard fin was instrumented with 24 pairs of unsteady pressure transducers at positions directly opposite to each other on each surface. The positions of the transducers are presented in Fig. 1 and their coordinates are given in Ref. 1. Calibration of the pressure transducers was accomplished by fitting a gas-tight glove over the entire fin "in-situ" on the model, thus subjecting each transducer to a common pressure from a nitrogen supply. A more detailed account of fin construction and instrumentation is available in Ref. 1.

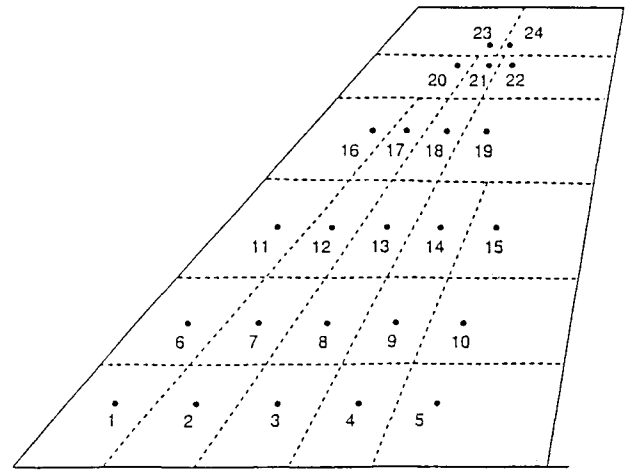

Fig. 1 Fin pressure transducer locations on wind-tunnel model.

Wind-tunnel run conditions, model angle of attack, and other parameters were acquired at 100 Hz using a PDP 11/73 computer-based wind-tunnel data system. This system also controlled the wind-tunnel operation and model position. Acquisition of the unsteady pressures on the starboard fin was undertaken using a microVax-based data acquisition system, with a sampling rate of 38.4 kHz per channel.

III. Full-Scale Aircraft Testing

In 1989, the Canadian Forces undertook a ground vibration test and a series of flight tests to determine the dynamic loading associated with the F/A-18 aft fuselage. Prime objectives included the measurement of structural response on the vertical fins, horizontal stabilators, and engine mountings, both with and without the LEX fence installed. The following sections briefly describe the test programs, whereas more complete descriptions are presented in Refs. 1 and 5.

A. Ground Vibration Test

A ground vibration test (GVT) was performed at AETE to establish the dynamic characteristics of the aft fuselage (notably the vertical fins) prior to flight testing. Testing was carried out on two different aircraft, one with a lightweight aft fuselage and one with a heavyweight (early production) aft fuselage.

During testing, the aircraft were supported on both undercarriage and jacks, with the weight equally distributed between them. The aircraft were fully fueled, and all weapon stations were clean, with wing and centerline pylons removed. Two separate methods were used to attach the shaker rods to the fin structure. Firstly, shaped boards were clamped to each side of each vertical fin, with the shaker rod connected to the boards. The other method used an aluminium pad that was bonded to the fin and then connected to the shaker rod.

For symmetric and antisymmetric excitation, two shakers were used, one on each fin. For the asymmetric modes, only one shaker on the port fin was used. In each case the frequency range of excitation was 0–100 Hz, peak excitation forces being 30 and 100 lb for the symmetric and asymmetric cases, respectively. Fin responses were measured using tip accelerometers and root strain gauges. The two primary modes, the fin first bending mode at approximately 15 Hz and the fin first torsional mode at approximately 45 Hz, were identified and studied in detail. Unfortunately, higher-order modes were not investigated.

The data acquired from the GVT test was also used for fine tuning the structural finite element Nastran model, which was used for calculations of vertical tail flutter.[6]

Table 1 Categorization of flight data from fence-on tests at 10,000 ft

AOA, deg	q, psf 40–75	75–125	125–175	175–225
$20 < AOA < 22$	—	—	8	8
$22 < AOA < 24$	—	—	9	11
$24 < AOA < 26$	—	9	9	9
$26 < AOA < 28$	11	9	28	9
$28 < AOA < 30$	10	10	10	10
$30 < AOA < 32$	10	10	—	—
$32 < AOA < 34$	10	10	—	—

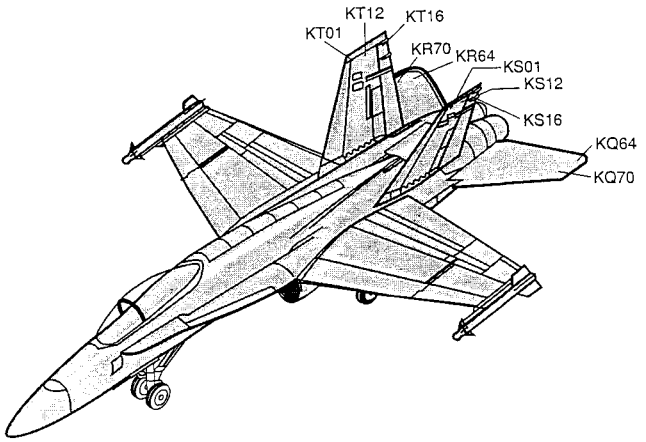

Fig. 2 Locations of flight test accelerometers.

B. Flight Tests

A total of 33 flight missions were flown on one of the aircraft that was used for the GVT. Flight maneuvers were performed that would take the aircraft through specified combinations of angle of attack and dynamic pressure, for both LEX fence on and off. However, only data obtained for LEX fence on is presented here. Test-point tolerances were restricted to ± 1 deg in angle of attack, ± 10 KCAS, and ± 1000 ft of the desired test conditions. Most test points were flown at 10,000 ft, whereas a few flights were flown at 30,000 ft.

Ten accelerometers were installed on the vertical fins and horizontal stabilators to measure the buffet response, as shown in Fig. 2. The transducers KS12 and KT12, whose coordinates were not documented in Ref. 1, are located at the same spanwise coordinate as KS01, KS16, etc., at approximately 64% of local chord. Accelerometer data was sampled at 606 Hz, and the flight test parameters (angle of attack, dynamic pressure, etc.) were sampled at 20 Hz. The data was then telemetered to the ground for real time monitoring and storage.

C. Flight Test Data Reduction

The vertical fin and horizontal stabilator data were analyzed at the IAR.[7]

For convenience, flight test data was subdivided into discrete ranges of both AOA and q. The data corresponding to a given combination of AOA/q was generally contained in one or more time intervals of contiguous data. During the flight test, flight parameters such as AOA, flight speed, test altitude, and flight time were continuously acquired, so that the discrete time intervals according to each AOA/q combination could be collected (together with the flight parameters for each time slice) for each flight mission.

Power spectral density (PSD) calculations were then performed on each individual time slice of data over 5 s in duration, together with a PSD of the overall time interval (i.e., all of the separate time slices concatenated). Table 1 represents the AOA/q combinations from the "fence on" missions flown at 10,000 ft, for which sufficient slices of contiguous data were available. The numbers in the boxes relate to the flight mission from which the data was acquired. It can be seen that the ranges of dynamic pressure are $40 < q < 75$, $75 < q < 125$, $125 < q < 175$, and $175 < q < 225$ psf, whereas the AOA data is divided into 2-deg intervals from $20 < AOA < 22$ deg to $32 < AOA < 34$ deg. Other AOA/q combinations were found to not contain the required amount of data. Selected PSDs of the flight data are presented later.

The flight data for the concatenated time slices was also reduced to the nondimensional buffet excitation parameter[8]:

$$\sqrt{nG(n)} = (2m\ddot{z}/\sqrt{\pi}qS)\sqrt{\zeta} \tag{1}$$

for the 15-Hz bending and 45-Hz torsional modes (for the transducers KS01, KT01, KS16, and KT16). The parameter represents the generalized force acting on the fin for each analyzed mode, although it is derived from the response (buffeting) measurements. The buffet excitation parameter has been used previously in various buffet studies.[9–11]

For each mode the acceleration time series was filtered using either a 15-Hz bandpass filter (passband from 10–20 Hz, stopband below 7 Hz and above 23 Hz) or a 45-Hz bandpass filter (passband from 38–52 Hz, stopband below 34 Hz and above 56 Hz). The rms levels for each mode were then derived from the resulting time series. The modal damping was determined using the half-power method, and modal masses were obtained from Nastran finite element analysis performed by Riedel.[6]

The matrix of analyzed flight data dictated the test points (AOA and Mach number) for the wind-tunnel study. For example, for the flight test condition $26 < AOA < 28$ deg and $75 < q < 125$ psf, wind-tunnel measurements were taken for AOA = 27 deg and $M = 0.31$ (the Mach number corresponding to $q = 100$ psf at 10,000 ft). In general, the difference between wind-tunnel and flight conditions was less than 10%.

IV. Buffet Prediction Method

A. Finite Element Model

Finite element analysis was performed to determine the fin structural dynamics for a range of natural modes, for the purposes of flutter analysis.[6]

The Nastran finite element model represented the fin as a cantilevered structure, with rotational springs at the fin root to model the flexibility of the root attachment to the airframe. Displacements of each panel were obtained by spline interpolation of the translations and rotations along the structural elastic axis of the fin, except for the rudder deflections, which were interpolated from the rudder elastic axis.

The first 10 modes were analyzed, and frequencies and node lines were well reproduced. The small variation between the measured symmetric, antisymmetric, and asymmetric mode shapes and frequencies in Table 7.11 of Ref. 5, shows that there is little coupling between the port and starboard fins. It is therefore appropriate to use the dynamic results from the cantilevered model.

B. Buffet Prediction Code

A buffet prediction code has been developed at the National Research Council, in conjunction with Carleton University,[12] to scale rigid model wind-tunnel data to a full-size elastic aircraft at flight conditions. The theory is presented in detail in Refs. 13 and 14, and only a brief summary is presented here.

For a Cartesian coordinate system fixed on the fin, as illustrated in Fig. 3, the total displacement of the fin may be expressed in terms of a set of normal coordinates $q_i(t)$:

$$y(x, z, t) = \sum_{i=1}^{N} \phi_i(x, z)q_i(t) \tag{2}$$

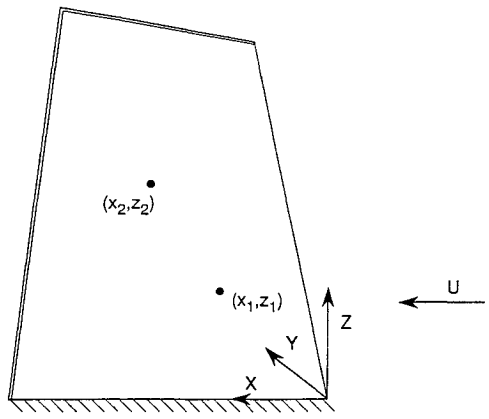

Fig. 3 Fin coordinate system.

The modal coordinate q_i is governed by the equation

$$M_i\ddot{q}_i + C_i\dot{q}_i + K_iq_i = l_i \tag{3}$$

l_i may be represented as the total force due to the forcing pressure distribution and aeroelastic terms as a result of the aerodynamic force induced by the deflection of the structure:

$$l_i = l_{iM} + l_{iD} \tag{4}$$

As a first approximation, only the terms due to the direct loading are studied. This loading induces response in the ith mode through the following expression:

$$l_{iD} = \int_{\text{area}} \int \phi_i(x, z)p(x, z, t)\,dx\,dz \tag{5}$$

where $p(x, z, t)$ is the instantaneous pressure across the fin.

The cross-spectral density (CSD) of each element of the generalized force is

$$S_{l_il_j}(\omega) = \int\int\int\int \phi_i(x_1, z_1)S_{p_1p_2}(x_1, z_1, x_2, z_2, \omega) \times \phi_j(x_2, z_2)\,dx_1\,dz_1\,dx_2\,dz_2 \tag{6}$$

where $S_{p_1p_2}(x_1, z_1, x_2, z_2, \omega)$ is the CSD between p_1 and p_2 at locations (x_1, z_1) and (x_2, z_2), respectively. By dividing the fin into 24 panels, each centered around a transducer location (Fig. 1), Eq. (6) is approximated to

$$S_{l_il_j}(\omega) = \sum_{b=1}^{24}\sum_{c=1}^{24} (A_b\bar{\phi}_{ib})S_{p_1p_2}(x_1, z_1, x_2, z_2, \omega)(A_c\bar{\phi}_{jc}) \tag{7}$$

$$\bar{\phi}_{ib} = \frac{1}{A_b}\int \phi_i(x, z)\,dA_b \tag{8}$$

For $b \neq c$, CSD terms are added, whereas if $b = c$, only PSD terms are added. Initially, the buffet prediction code assumed that the pressure over each panel exhibited perfect spatial correlation inside the panel, and zero spatial correlation with every other panel (i.e., CSD terms are zero).[15] The current version incorporates CSD terms to account for correlation of pressure over the fin surface.

Introducing a complex $H_i(\omega)$ for each mode, where

$$H_i(\omega) = \frac{1}{1 - (\omega/\omega_{n_i})^2 + 2i\zeta_i(\omega/\omega_{n_i})} \tag{9}$$

the spectra of $Q_i(\omega)$ and $S_i(\omega)$ are related by

$$Q_{ij}(\omega) = H_i^*(\omega)S_{l_il_j}(\omega)H_j(\omega) \tag{10}$$

where the superscript asterisk denotes the matrix transpose. The PSD of the displacement at any point on the fin is, therefore,

$$S(x, z, \omega) = \sum_i^N \sum_j^N \bar{\phi}_i(x, z)Q_{ij}(\omega)\bar{\phi}_j(x, z) \tag{11}$$

The displacement is then converted to acceleration by multiplying by ω.[4]

Initially, the wind-tunnel data is read in for each transducer pair, the differential pressure across the fin is derived, and the PSD and relevant CSDs are calculated [using a fast Fourier transform (FFT) length of 16,384, and approximately 20 ensemble averages], and written to file. Then the spectra are read and scaled in terms of reduced frequency. The transfer function for each fin mode is derived and the contribution by each term towards the generalized displacement matrix is calculated. When the $S_{l_il_j}$ matrix is full, the modal displacements for the chosen location on the fin are interpolated from the Nastran analysis, and Eq. 11 is used to obtain the PSD of displacement.

Previous buffet studies[4] have used a doublet lattice code to simulate the effect of structural deflection on the vortex/fin interaction so that values of aerodynamic damping and stiffness could be included in Eq. (3). For the present approach the effect was simulated by incorporating aerodynamic damping values derived from the Nastran flutter model into Eq. (3), without using the doublet lattice in the actual code.

V. Presentation and Discussion of Results

A. Buffet Prediction Method

Results from the initial buffet prediction code (where zero spatial correlation between panels was assumed) gave significant underpredictions of the full-scale response.[15] Also, a study assuming 100% spatial correlation[16] yielded significant overpredictions. Therefore, it was decided that a form of partial pressure correlation was needed for more accurate predictions. Subsequent tests incorporating CSD terms into the prediction model gave a better prediction, implying significant correlation between neighboring panels. Hence, a study was undertaken to establish the degree of pressure correlation on the fin surfaces, so that the prediction technique could be further refined. The approach of Lee and Tang[17] was employed to determine the scale of the broadband eddies. The rows of transducers used for the analysis were transducers 1–5, 6–10, 11–15, and 16–19 in the streamwise direction, and 1–16, 2–17, 3–18, and 4–19 in the spanwise direction (see Fig. 1). The eddy scale was defined as the distance from a reference transducer in either the streamwise or spanwise directions, for which the peak cross correlation function had decreased to l/e of the value at the reference transducer.[17]

The variation of the eddy scale for both faces of the fin is presented in Figs. 4 and 5 for the streamwise direction. Even though there is a degree of scatter present in the data, important trends can be established. For the outboard face of the fin (Fig. 4) the variation of the eddy scale is small. However for the inboard face of the fin (Fig. 5) it can be seen that the eddy scale increases with AOA. Previous studies of F/A-18 tail buffet[4] have found that the inboard surfaces of the fins experience the majority of the forcing pressure distribution, whereas the outboard surface experiences less excitation. The values from Ref. 17 are also plotted on these figures and are in the correct range. No significant Mach number effects were encountered.

Also indicated on the graph are average panel dimensions. It can be seen that for low AOAs (AOA = 21 deg) zero extra panels should be incorporated into the prediction model, i.e., PSD terms only. For 23 ≤ AOA ≤ 29 deg it is suggested that one extra panel be used for all directions. Therefore, panel 7, e.g., would be influenced by panels 1, 2, 3, 6, 8, 11, 12, and 13 (see Fig. 1). For AOA ≥ 31 deg, two extra panels

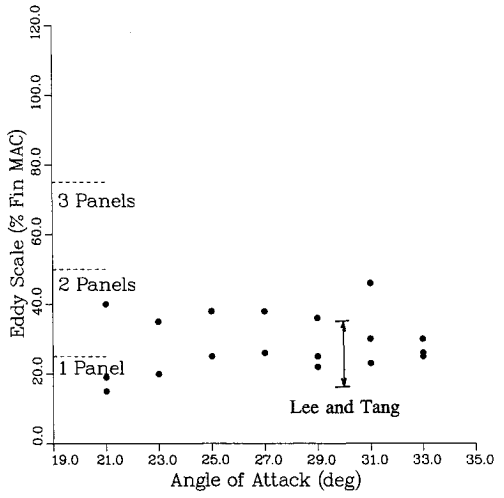

Fig. 4 Variation of broadband eddy scale on fin outboard surface in the streamwise direction.

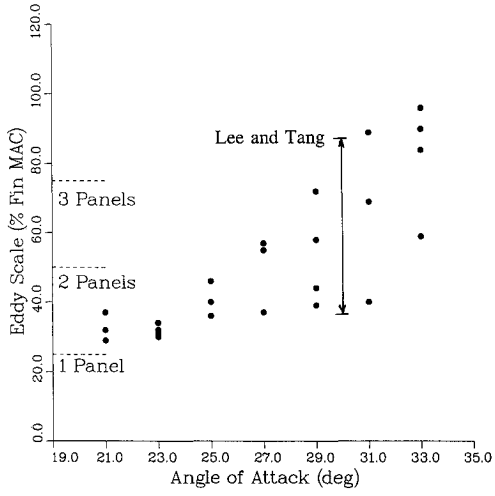

Fig. 5 Variation of broadband eddy scale on fin inboard surface in the streamwise direction.

should be added to the prediction to account for the increase in pressure correlation on the inboard face of the fin.

The results of the buffet prediction code (expressed as the PSD of acceleration) are presented together with the corresponding flight test spectra in Figs. 6–8 for the transducers KS01/KT01, KS12/KT12, and KS16/KT16, respectively. The flight test conditions correspond to $28 < \text{AOA} < 30$ deg and $125 < q < 175$ psf, and it should be noted that since k is used, the PSD scale is g^2/k. The two main natural modes of interest are the first two peaks, corresponding to the fundamental bending mode at approximately 15 Hz and the fundamental torsional mode at approximately 45 Hz. The other two significant modes are the second bending mode at approximately 66 Hz and a higher mode at approximately 95–100 Hz, whose mode shape has not been analyzed. Since these higher-order modes were not studied during the GVT it is difficult to establish their modal characteristics.

The solid curve represents the initial prediction model (PSD terms only), whereas the chain-dotted line represents the inclusion of CSD terms (one extra term in both streamwise and spanwise directions). It can be seen that the inclusion of CSD terms increases the accuracy of the buffet prediction code (in terms of the primary modes and the overall rms acceleration) and gives good comparisons to the flight test data. For the transducer KS01 both primary bending and torsional modes are prominent, as are the higher modes, whereas for KS12 the 15 Hz bending mode is dominant due to the transducer's

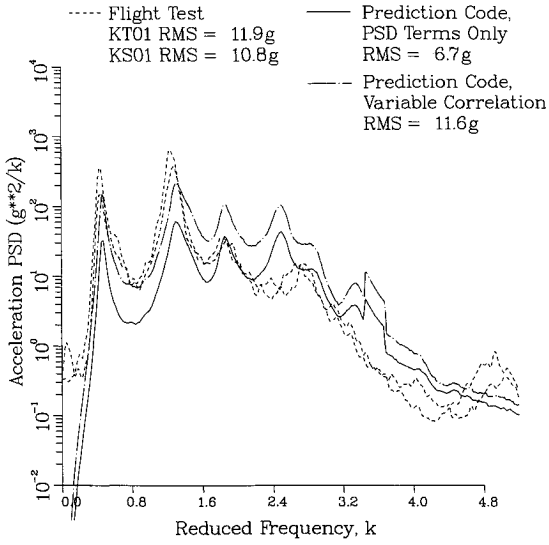

Fig. 6 Comparison of spectra between prediction and flight test for KS01, $125 < q < 175$, $28 < \text{AOA} < 30$ deg.

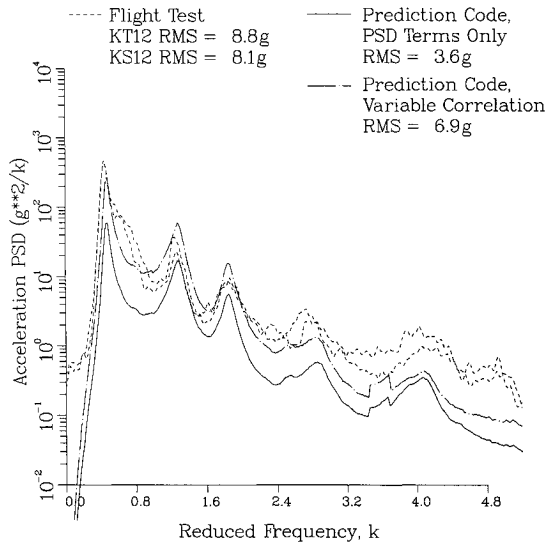

Fig. 7 Comparison of spectra between prediction and flight test for KS12, $125 < q < 175$, $28 < \text{AOA} < 30$ deg.

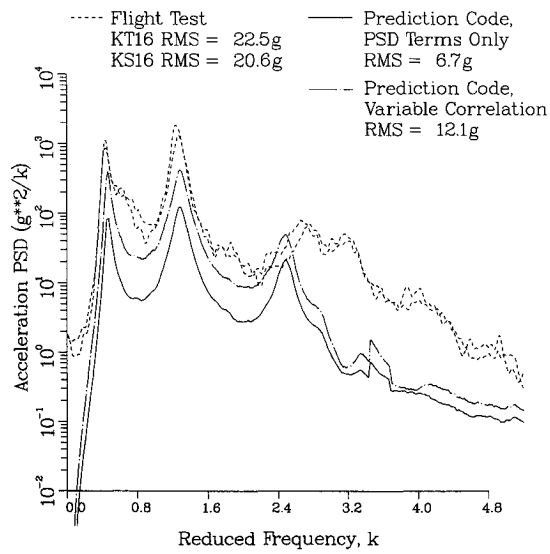

Fig. 8 Comparison of spectra between prediction and flight test for KS16, $125 < q < 175$, $28 < \text{AOA} < 30$ deg.

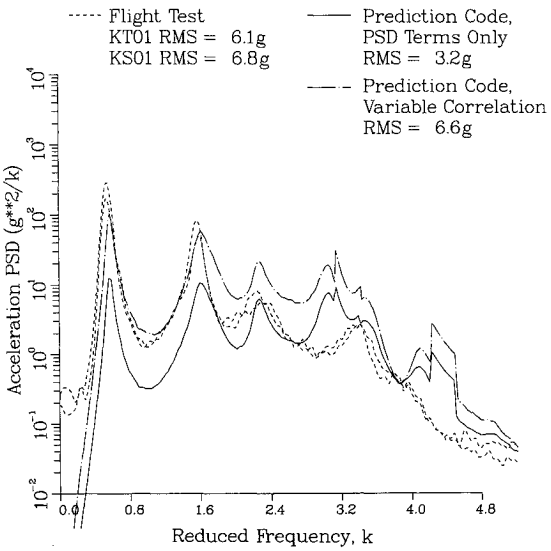

Fig. 9 Comparison of spectra between prediction and flight test for KS01, 75 < q < 125, 30 < AOA < 32 deg.

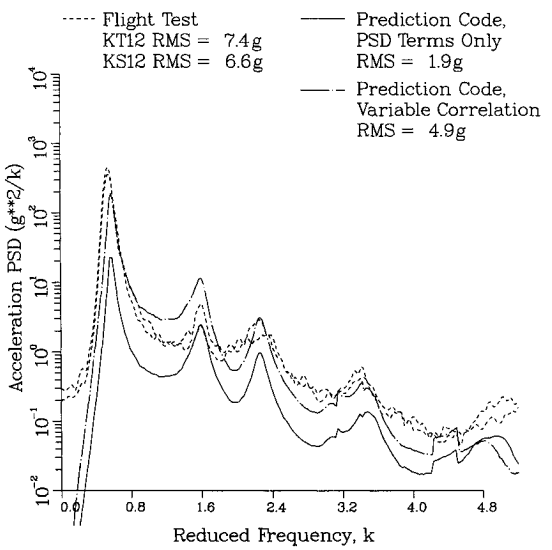

Fig. 10 Comparison of spectra between prediction and flight test for KS12, 75 < q < 125, 3 < AOA < 32 deg.

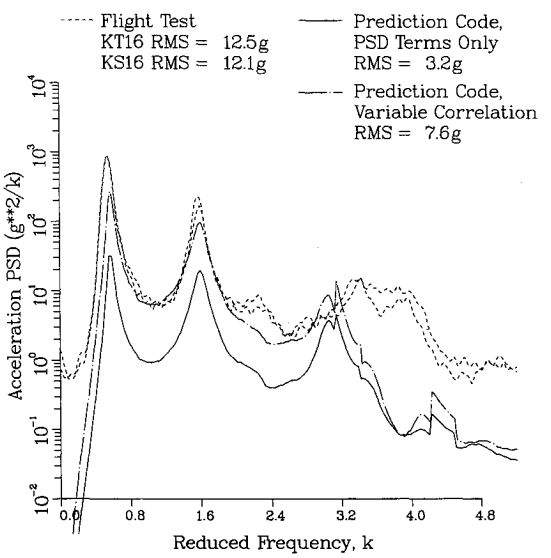

Fig. 11 Comparison of spectra between prediction and flight test for KS16, 75 < q < 125, 30 < AOA < 32 deg.

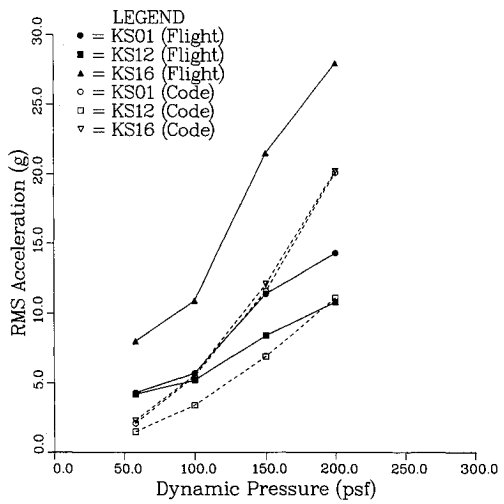

Fig. 12 Variation of rms acceleration with q, 28 < AOA < 30 deg.

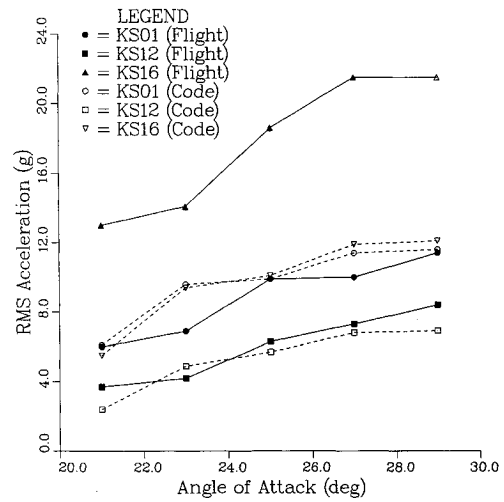

Fig. 13 Variation of rms acceleration with AOA, 125 < q < 175 psf.

proximity to the fin torsional axis. Peak responses in the two primary modes are predicted for the transducer KS16, in accordance with the flight test data. However, the response at KS16/KT16 is underpredicted to a greater degree than the responses at KS01/KT01 and KS12/KT12. This was seen to occur for most test points. Since the differences between the results for the various transducers are only due to the mode shapes calculated at the transducer locations (as the contributions to the generalized force matrix $S_{ij,l}$ are common), this inconsistency may be due to inaccuracies in the Nastran model or to differences between the fin structure properties and the Nastran model.

Figures 9–11 compare code and flight spectra for the flight conditions 30 < AOA < 32 deg and 75 < q < 125 psf, using both the initial prediction code and the code incorporating CSD terms (two extra terms in this case, due to the increase in the broadband eddy scale). The curves incorporating CSD terms all give better predictions compared to the initial prediction, including the primary modes and the overall rms acceleration.

Figures 12 and 13 show the variation in rms acceleration for the AOA range 28 < AOA < 30 deg and the q range 125 < q < 175, respectively, for both flight test and code. It can be seen that the code gives fair comparisons with flight test.

B. Buffet Excitation Parameter

The flight data was also analyzed to obtain the buffet excitation parameter in order to compare the F/A-18 tail buffet

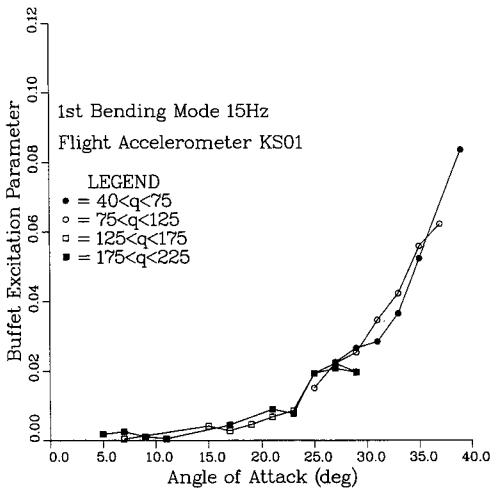

Fig. 14 Variation of buffet excitation parameter with AOA for accelerometer KS01 at fundamental bending mode 15 Hz.

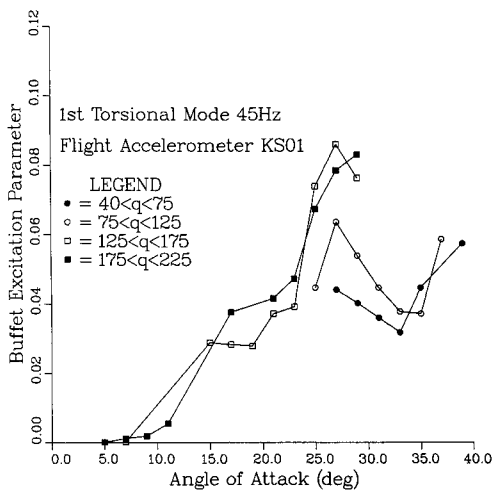

Fig. 15 Variation of buffet excitation parameter with AOA for accelerometer KS01 at fundamental torsional mode 45 Hz.

phenomenon with the results from various wind-tunnel programs performed on different aircraft.

Figures 14 and 15 show the variation of buffet excitation parameter vs AOA for the transducer KS01 for both primary modes. It can be seen that buffet onset occurs at a lower AOA for the torsional mode and that the torsional response peaks in the region $26 < \text{AOA} < 30$ deg. The bending response still increases up to AOA = 38 deg, and since this is the maximum AOA for which sufficient flight data was available, the point of maximum bending is unknown. Peak levels are around 0.10, which is much larger than the measure of "heavy" wing buffet suggested by Mabey[8] (0.003), and the wind-tunnel measurements of fin buffet performed by Mabey[18] (0.037) and Zan[9] (0.06). This may be due to the larger levels of total damping obtained during flight conditions (up to 15% in some cases). The curves for the bending mode do not show any dependence on flight dynamic pressure, whereas this is the case with the torsional curves. This anomaly may be the result of the short record lengths obtained during flight test, together with the larger torsional rms values.

The generalized force (normalized with respect to q) for each primary mode was calculated from the wind-tunnel data by weighting the differential pressure at each panel with the corresponding mode shape for that panel:

$$l_i' = \frac{1}{q} \sum_{b}^{24} p_b \bar{\phi}_{ib} A_b \qquad (12)$$

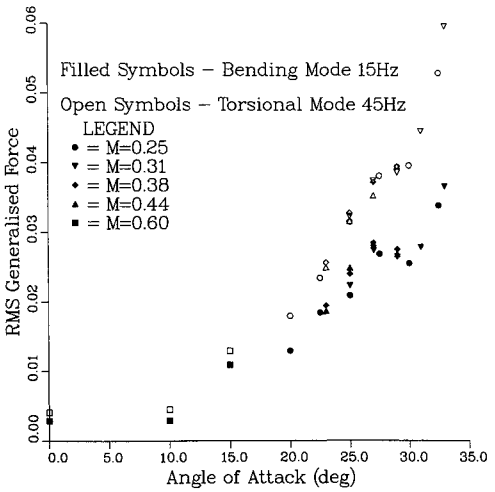

Fig. 16 Variation of rms generalized force (normalized with respect to q) with AOA.

Figure 16 shows the broadband rms variation of the generalized force vs AOA for Mach number range 0.25–0.6. Although the terms in Eq. (12) are weighted with each panel mode shape, the rms values are broadband, and therefore, quantitative comparisons with Figs. 14 and 15 cannot be deduced. It can be seen that buffet onset is well defined at AOA $\approx$ 10 deg and that the torsional weighting yields larger rms values. A slight dip in the curves for $26 < \text{AOA} < 30$ deg may correlate with decreased torsional responses, although this has not been confirmed. Both curves then continue to rise, but the AOA of peak rms generalized force is unknown due to limitations in the model AOA range. No significant dependence on Mach number was observed for the Mach number range tested.

VI. Conclusions

In general, the buffet prediction code gives good comparisons with the flight data, once the influence of pressure correlation has been addressed. It was found that the scale of the broadband eddies increased for increasing AOA, so that extra CSD terms were necessary in the prediction model.

The flight data was reduced to the nondimensional buffet excitation parameter, for each primary mode. It was found that buffeting in the torsional mode occurred at a lower angle of attack and at larger overall levels compared to the fundamental bending mode. The magnitudes of the parameter are at least one order of magnitude larger than a suggested limit for heavy wing buffeting.

Acknowledgments

The first author would like to thank the National Research Council of Canada for its award of a G-7 Summit Fellowship. The financial support from the Institute for Aerospace Research, Department of National Defence and the Natural Sciences and Engineering Research Council of Canada is gratefully received. The authors also acknowledge the assistance of staff at the High Speed Aerodynamics Laboratory, notably M. Plosenski, F. C. Tang, and D.F. Hawken.

References

[1]Lee, B. H. K., Brown, D., Zgela, M., and Poirel, D., "Wind Tunnel Investigation and Flight Tests of Tail Buffet on the CF-18 Aircraft," CP 483, AGARD, 1990 (Paper 1).

[2]Rao, D. M., Puram, C. K., and Shah, G. H. "Vortex Control for Tail Buffet Alleviation on a Twin Tail Fighter Configuration," Society of Automotive Engineers 892221, Sept. 1989.

[3]Lee, B. H. K., and Brown, D., "Wind Tunnel Studies of F/A-18 Tail Buffet," *Journal of Aircraft*, Vol. 29, No. 1, 1992, pp. 146–152.

[4]Ferman, M. A., Patel, S. R., Zimmerman, N. H., and Gestern-

korn, G. "A Unified Approach to Buffet Response of Fighter Aircraft Empennage," CP 483, AGARD, 1990 (Paper 2).

[5]Zgela, M. B., "Measurement of Fin Attachment Strains on Two CF-18 Aircraft During Ground Vibration Tests," Aerospace Engineering and Test Establishment, AETE Rept. 85/53, Cold Lake, AB, Canada, Sept. 1989.

[6]Riedel, F., private communication, Logiscan Inc., Dorval, PQ, Canada.

[7]Hawken, D. F., "Analysis of Buffet Response from AETE Test Flights," Inst. for Aerospace Research TR LTR-HA-91, National Research Council, Ottawa, ON, Canada, March 1993.

[8]Mabey, D. G., "Some Aspects of Aircraft Dynamic Loads Due to Flow Separation," AGARD R-750, May 1988.

[9]Zan, S. J. "Measurements of Wing and Fin Buffeting on the Standard Dynamics Model," Inst. for Aerospace Research TN AN-76, National Research Council, Ottawa, Ontario, Canada, May 1993.

[10]Bean, D. E., Greenwell, D. I., and Wood, N. J., "Vortex Control Technique for the Attenuation of Fin Buffet," *Journal of Aircraft*, Vol. 30, No. 6, 1993, pp. 847–853.

[11]Bean, D. E., and Wood, N. J., "An Experimental Investigation of Twin Fin Buffeting and Suppression," AIAA Paper 93-0054, Jan. 1993.

[12]Black, C. L., "CF-18 Tail Buffet Prediction Based on Rigid Model Pressure Data," M.S. Thesis, Carleton Univ., Ottawa, ON, Canada, 1993.

[13]Lee, B. H. K., "Aeroelastic Response of an Aircraft Wing to Random Loads," National Aeronautical Establishment TR LR-613, National Research Council, Ottawa, ON, Canada, April 1983.

[14]Lee, B. H. K., "A Method for Predicting Wing Response to Buffet Loads," *Journal of Aircraft*, Vol. 21, No. 1, 1984, pp. 85–87.

[15]Bean, D. E., and Lee, B. H. K., "Correlation of Wind Tunnel and Flight Test Data for F/A-18 Vertical Tail Buffet," AIAA Paper 94-1800, June 1994.

[16]Ashley, H., Rock, S. M., Digumarthi, R., Chaney, K. and Eggers, A. J., "Active Control for Fin Buffet Alleviation," Wright–Patterson Rept. WL-TR-93-3099, Jan. 1994.

[17]Lee, B. H. K., and Tang, F. C., "Characteristics of the Surface Pressures on a F/A-18 Vertical Fin Due to Buffet," *Journal of Aircraft*, Vol. 31, No. 1, 1994, pp. 228–235.

[18]Mabey, D. G., and Pyne, C. R., "Reduction of Fin Buffeting by Tangential Blowing on the Leading Edge of a Delta Wing," Defence Research Agency TM 2215, May 1991.

Recommended Reading from the AIAA Education Series

The Fundamentals of Aircraft Combat Survivability: Analysis and Design

Robert E. Ball

An extensively illustrated text that presents the fundamentals of the aircraft combat survivability design discipline as defined by the DoD Military Standard issued in 1981. It provides the history of, the concepts for, and the assessment methodology and the design technology for the non-nuclear combat survivability analysis and design of fixed- and rotary-wing aircraft and missiles. Of critical interest to anyone involved in the design and development of military aircraft or airborne weapon systems, the book also will be useful to weapon systems effectiveness analysts.

1985, 398 pp, illus, Hardback, ISBN 0-930403-02-9
AIAA Members $42.95, Nonmembers $57.95
Order #: 02-9 (830)

Place your order today! Call 1-800/682-AIAA

AIAA
American Institute of Aeronautics and Astronautics

Publications Customer Service, 9 Jay Gould Ct., P.O. Box 753, Waldorf, MD 20604
FAX 301/843-0159 Phone 1-800/682-2422 8 a.m. - 5 p.m. Eastern

Sales Tax: CA residents, 8.25%; DC, 6%. For shipping and handling add $4.75 for 1-4 books (call for rates for higher quantities). Orders under $100.00 must be prepaid. Foreign orders must be prepaid and include a $20.00 postal surcharge. Please allow 4 weeks for delivery. Prices are subject to change without notice. Returns will be accepted within 30 days. Non-U.S. residents are responsible for payment of any taxes required by their government.